










A comprehensive evaluation of heavy metals removal from battery industry wastewaters by applying bio-residue, mineral and commercial adsorbent materials

Caroline Ribeiro^{1,*} , Fabiano Bisinella Scheufele² , Fernando Rodolfo Espinoza-Quiñones¹ , Aparecido Nivaldo Módenes¹ , Melissa Gurgel Adeodato Vieira³ , Alexander Dimitrov Kroumov⁴ , and Carlos Eduardo Borba¹ 

¹ Department of Chemical Engineering, Post graduate Program, West Parana State University, UNIOESTE, Campus of Toledo, Rua da Faculdade 645, Jd. La Salle, Toledo, PR 85903-000, Brazil

² Department of Engineering and Exact Sciences, Federal University of Paraná, Sector of Palotina, Pioneiro St. 2153, Palotina, PR 85950-000, Brazil

³ School of Chemical Engineering, State University of Campinas, UNICAMP, Cidade Universitária ZeferinoVaz, P.O. Box 6066, Campinas, SP 13081-970, Brazil

⁴ Department of Applied Microbiology, Division "Microbial Synthesis and Ecology" The "Stephan Angeloff" Institute of Microbiology, Bulgarian Academy of Sciences, Bl. 26, 1113 Sofia, Bulgaria

Received: 10 December 2017

Accepted: 14 February 2018

Published online:
26 February 2018

© Springer Science+Business
Media, LLC, part of Springer
Nature 2018

ABSTRACT

We present a feasibility study of different adsorbent materials, namely residual fish scales biosorbent (FS), mineral dolomite (DL) and commercial resin (CR) in the heavy metals removal in multicomponent solution based on the properties of a real effluent from automotive battery recycling industry. Considering the effluent complex characteristics, the materials were assessed aiming to provide not only the heavy metals removal, but also the effluent neutralization and lower sludge generation. For this, all the studied materials were physicochemically and morphologically characterized with the aim of understanding the mechanisms involved in the process. Further, the elemental compositions of the solid and liquid phases generated from each treatment process were assessed by X-ray fluorescence spectrometry. The effluent presented highly acidic characteristics and heavy metals above the legislated limits for discharge (Fe, Zn and Pb). Each adsorbent material followed different mechanisms which led to dissimilar removal and neutralization capacities. The CR showed remarkable heavy metals removal capacity governed by an ion exchange mechanism; conversely, it did not show a neutralization effect. In contrast, FS and DL presented lower removal capacities by complex simultaneous phenomena (ion exchange, precipitation and/or complexation), but a great neutralization potential related to leaching of alkaline constituents. When sludge generation is considered as a key factor, mitigation and enhancement of treated effluent quality could

Address correspondence to E-mail: caroline-rib@hotmail.com

alternatively be addressed by employing the materials in hybrid processes. Hence, the associated use of such materials could be viable yet very challenging for both neutralization and removal of heavy metals from the battery effluent.

Introduction

Lead–acid automotive batteries are the most widespread battery system in the world scenario. Because of their extensive use, the destination of lead–acid batteries is a major environmental concern due to the high metal toxicity [1] and extreme acidic characteristics. Long-term exposure of humans to these metals can cause nephropathy or a decrease in the performance of nervous systems, and it can significantly affect brain development in children [2–4].

Although the traditional recycling technologies of scrap metals through foundries are relatively consolidated, the pollution caused by such materials is still relevant [5]. However, deficiencies in the management infrastructure and logistics of these materials and inefficient treatment processes can be commonly perceived, which cause secondary pollution during the recycling process.

Though not limited to but taking the case of Brazil as an example, the environmental monitoring and regulatory agencies have a limited capacity to control the polluting activities. In this context, different studies report that lead–acid battery recycling processes are commonly performed in an environmentally inadequate or inefficient way. In many cases, the companies that carry out these activities have precarious facilities without pollution control equipment [6, 7]. In 2010 the National Solid Waste Policy (PNRS—*Política Nacional de Resíduos Sólidos* [in Portuguese]) was implemented in Brazil. Throughout the regulations, reverse logistics and shared responsibility were some of the highlights of this regulatory framework, in which manufacturers, importers, distributors and dealers of batteries and accumulators are required to structure and to implement reverse logistics systems. Thus, the product, after its use by the consumer, must be returned, independent of the public service of urban cleaning and solid waste management (according to Art. 33—PNRS).

Among the most popular technologies that prevail in the treatment of these effluents, methods such as chemical precipitation, ion exchange, filtration,

decantation, neutralization, electrochemical treatment and evaporative recovery can be highlighted [5]. However, depending on the wastewater characteristics, these processes may have significant drawbacks such as incomplete metal removal, demand for expensive equipment and energy-intensive monitoring systems and the generation of secondary residues, namely toxic sludge and other waste released into the air and soil that require further treatment steps. Chemical precipitation stands out as one of the most widely used treatment methods in industrial effluents due to its low cost and simplicity. Nevertheless, chemical precipitation has the disadvantages of generating large volumes of complex sludge and having low efficiency for treatment of highly diluted metal solutions [1, 8].

Given the background, more effective technologies that can reduce concentrations of heavy metals to environmentally acceptable levels at affordable prices are needed [1, 5, 9, 10]. Sorption processes have been extensively used as alternative methods in the treatment of heavy metals, aiming for high adsorption capacity and cost-effective materials [11, 12]. Several adsorbent materials have been studied as reported elsewhere, especially abundant and locally available ones such as rock minerals [13–17], agricultural and industrial wastes [8, 18] or even commercial materials such as silica gel, resins and zeolites [19–21].

Despite the large number of heavy metals adsorption studies reported in the literature, there is a lack of investigations of the species released from the adsorbent materials to the liquid phase as well as a comprehensive evaluation of the water quality and the sludge generated during the process. In addition, a comparison of different sources for the same effluent may contribute in the comprehension of the mechanisms involved in the treatment of such a complex system using each material, since several phenomena may take place simultaneously in the process.

In view of the above-highlighted drawbacks in the analyzed research area, in this paper we present a feasibility study of three types of adsorbent materials (i.e., biosorbent, mineral and commercial resin) in the

removal of heavy metals from a multicomponent solution based on the properties of a real effluent from automotive battery recycling industry. For this, a characterization of the effluent from an industrial complex was performed. In addition, an evaluation of the composition and quality of both the treated effluent and the generated sludge was conducted, wherein all the materials, as well as the solid and liquid phases of the process, were physicochemically and morphologically characterized aiming at a better understanding of the mechanisms involved in the process.

Materials and methods

Adsorbent materials

In this work, adsorbent materials from different sources with different characteristics were investigated as heavy metals-removing agents, as follows:

- (1) *Biomaterial* The biomaterial used was the *Oreochromis niloticus* fish scale (FS), which is an abundant residue of the fish slaughterhouse industry. In rare situations, this type of residue is adequately destined and/or is used in noble applications, which remains a persistent and significant issue in the segment. The FS was kindly supplied by a company located in the western region of Paraná.
- (2) *Mineral material* The mineral material employed was dolomitic lime (DL), which is the main alkaline agent used on a large scale for the treatment of water and effluents. The DL presents excellent physicochemical characteristics combined with its cost-effectiveness and ease of acquisition. In this study, dolomitic lime was generically treated as “mineral” material because, due to its extensive use in effluent treatment, it may change in composition and degree of purity depending on the source.
- (3) *Commercial material* The commercial material investigated in this study was the Amberlite IR120[®] resin, manufactured by Rohm and Haas Company, which is a microporous cationic resin (CR). The CR consists of a divinylbenzene styrene copolymer matrix with sulfonic acids as functional groups (R-SO₃H) with Na⁺ as the counterion. The resin particles are of spherical

shape, with an average size of 0.5 mm, and have high physical, chemical and thermal stability.

The three studied materials (i.e., mineral, fish scale and resin) were characterized in terms of physicochemical properties by applying the following analytical techniques: elemental analysis, point of zero charge—pHpzc, Fourier transform infrared spectroscopy (FTIR) analysis and scanning electron microscopy with energy-dispersive X-ray analysis (SEM–EDX). The material characterization was performed to evaluate physicochemical and morphological properties of the materials, according to its specificity, before and after the process.

Note It must be highlighted that the term “adsorbent materials” must be cautiously addressed since other physicochemical phenomena other than strictly surface adsorption may take place concomitantly, such as adsorption, ion exchange, surface complexation and precipitation [22, 23]. Thus, a much more complex mechanism is generally responsible for such processes.

Characterization of the industrial wastewater

Initially, aiming to investigate the characteristics of the battery recycling industrial wastewater and to assess its possible oscillations in the process, a total of 16 samples were collected from the industrial complex during a 50-day period, according to the company’s determination. The collected samples were analyzed in terms of the elemental composition and pH value, as both the heavy metals concentrations and the extreme acidity values lead to the harmful character of such effluents.

Elemental characterization and pH evaluation of the industrial wastewater

The pH values of the collected samples from the industrial site were measured by GEHAKA pH meter model PG1800, with a glass electrode. For the quantification of the heavy metals in the industrial wastewater, an elemental characterization was performed by applying total reflection X-ray fluorescence spectrometry (TXRF) analysis using a benchtop portable spectrometer (S2 PICOFOX, Bruker AXS Microanalysis GmbH).

The samples were prepared according to the methodology proposed by Espinoza-Quinones et al. [24] in which before sample preparation, the quartz glass disks (30 mm diameter and 3 mm thickness) were subject to a specific cleaning which was done to avoid contamination. Aiming to obtain a thin dried spot of the residue on the surface of the quartz disks for the TXRF analysis, the samples were prepared in Eppendorf microtubes with a capacity of 2 mL, in which were added 660 μL real effluent sample, 330 μL solution of 6 mol L^{-1} NaOH, for the sample's neutralization, and a 10- μL aliquot of a Gallium standard solution as an internal standard. Hence, 5 μL of each sample was pipetted onto the center of the quartz glass disks and dried on the disks in a laminar flow hood at room temperature. The used micropipettes were carefully calibrated. For the solid samples (post-treatment sludge), 30 mg of the sample (granulometry < 50 μm) was added to Eppendorf microtubes along with 2.5 mL of TritonTM X-100 (Sigma-Aldrich) at 1% (v/v) and 100 μL of the Gallium standard solution.

Point of zero charge (pH_{pzc})

The point of zero charge (pH_{pzc}) of the three adsorbent materials was determined by the “drift method” [25], wherein 50 mL solutions containing 0.01 mol L^{-1} NaCl were prepared in Erlenmeyer flasks in a pH range from 1 to 12 by adjusting with 0.01 mol L^{-1} NaOH and 0.01 mol L^{-1} HCl. In each test, 100 mg of the adsorbent material was added and kept for 24 h at which time the equilibrium pH value of the samples was measured. According to the methodology, the graphical interpretation of the $\text{pH}_{\text{initial}}$ vs. pH_{final} indicates the point of zero charge, which corresponds to the point where the pH variation is zero.

Fourier transform infrared (FTIR) spectroscopy

The surface functional groups of the adsorbent were analyzed by FTIR spectroscopy (model—FTIR/NIR spectrum, PerkinElmer, Frontier). The same analysis was performed for the adsorbent materials after the process, aiming to identify possible interactions between the heavy metals and the sites of the adsorbent. FTIR spectra were obtained by diffuse reflectance in the mid-infrared region (between 4000 and 650 cm^{-1}) at a resolution of 1 cm^{-1} by accumulating 16 scans. The infrared spectra were baseline-

corrected and normalized based on each respective spectrum area.

X-ray diffraction (XRD) analysis

In order to complement the FTIR technique and to characterize the crystalline structure of the materials as well as to identify any possible changes after the process, XRD analyses were performed in the materials before and after the treatment process. For this, the XRD patterns were obtained by using a Bruker diffractometer (D2-PHASE) operating in the continuous scanning mode with Cu-K α radiation (1.5418 Å) and nickel filter at a voltage of 30 kV and current of 10 mA. A scanning speed in 2θ of 0.02° min^{-1} and step time of 1.0 s were used in the range of 5° up to 80°. The solid samples were ground in order to achieve a fine powder with granulometry under 270 mesh (\approx 50 μm).

Scanning electron microscopy–energy-dispersive X-ray spectroscopy (SEM–EDX)

SEM micrographs from the materials before and after the treatment process were obtained by a scanning electron microscope, Tescan Vega 3, and further, the morphological modifications in the solid materials were investigated. The samples were previously covered with a thin layer of gold by a metallizer and then fixed in a sample holder by a carbon tape. In addition to the images, the equipment contained an energy-dispersive X-ray spectroscopy (EDS) system (Penta FET Precision—Oxford) which allowed a semiquantitative evaluation of the chemical composition.

Kinetic tests

In order to compare the removal capacity of each evaluated material, kinetic adsorption tests were performed. The metal solutions were prepared by diluting each heavy metal salt (i.e., iron, zinc and lead) with a deionized water solution, previously adjusted to a pH equal to 1, according to the typical concentration and pH values observed in the characterization of the industrial effluent. All the used salts were of analytical reagent grade. The kinetic assays consisted of adding 20 g of each adsorbent material to 1 L of the heavy metal multicomponent solution. The experiments were conducted in batch

mode by using a stirred tank with controlled temperature and stirring speed (25 °C and 90 rpm) for 24 h of process time. The temperature and pH values of the system were monitored throughout the time of the experiment, and periodic aliquots were collected. Further, the samples were vacuum-filtered with 0.45- μm cellulose acetate membranes, and the remaining metal concentrations in solution were determined by TXRF according to the methodology described in “Elemental characterization and pH evaluation of the industrial wastewater” section. In addition, the adsorbent materials after the removal tests (i.e., solid phase) were collected, dried and appropriately stored for subsequent characterizations. The percentage of removal (% *R*) was determined by applying Eq. (1).

$$\%R = 1 - \frac{C_f}{C_i}, \quad (1)$$

where C_i stands for the initial concentration of the metal species (mg L^{-1}) and C_f is the concentration of the metal species in the solution after the process (mg L^{-1}).

Results and discussion

Characterization of the industrial wastewater

Periodic sampling of the industrial wastewaters was performed for a 50-day period, and then the samples were characterized in terms of their elemental concentration, mainly for heavy metals (TXRF analysis). The pH value of the samples was measured as well. Table 1 shows the quantitative elemental characterization of crude effluent. In the crude effluent, heavy metal concentrations in ppm magnitude were observed, wherein the highest concentration values were determined to be for Fe, Zn and Pb followed by other heavy metals with much lower concentrations (Cr, Cu and Ni $< 2 \text{ mg L}^{-1}$). The values of the standard deviation for the metal concentrations were elevated, most probably associated with the common oscillations from the process entrance. These variations can also be observed in the inferior and superior limits (IL and SL values) (see Fig. 1).

The pH profile of the battery recycling industrial wastewater, which presented an average value of 1 ± 0.2 , is shown in Fig. 1a. The Brazilian entity that controls and regulates the discharge of wastewater

(CONAMA) [26] demands that the pH of an industrial effluent discharge must be between 5 and 9. In addition, the concentration profiles of the heavy metals (Fe, Zn and Pb) observed in higher concentrations in the crude effluent, according to Table 1, are shown in Fig. 1b. A great variability during the sampling period was observed, due to the above-mentioned intrinsic oscillations of the process, especially for Fe. Based on the values presented in Table 1 for the limits on concentrations of heavy metals (CONAMA) [26], one may notice that the values observed in the effluent characterization are above the release standards.

From the characterization results, an effluent that is extremely acidic and highly contaminated with heavy metals was verified. Hence, an efficient and adequate treatment is required in order to achieve the reuse and/or disposal standards required by legislation. Several conventional methods are commonly employed, for instance, chemical precipitation or coagulation (e.g., aluminum sulfate); however, these methods may present some drawbacks, such as substantial sludge generation, which can increase the overall treatment process costs related to disposal. In addition, these methods are generally not suitable for the treatment of effluent with low metals concentration.

Characterization of the adsorbent materials

In order to evaluate the chemical and physical stability of the adsorbent materials as well as to clarify our understanding of the phenomena involved in the process, a comprehensive characterization of the studied materials in terms of pH_{pzc} , SEM–EDX, FTIR and XRD was performed.

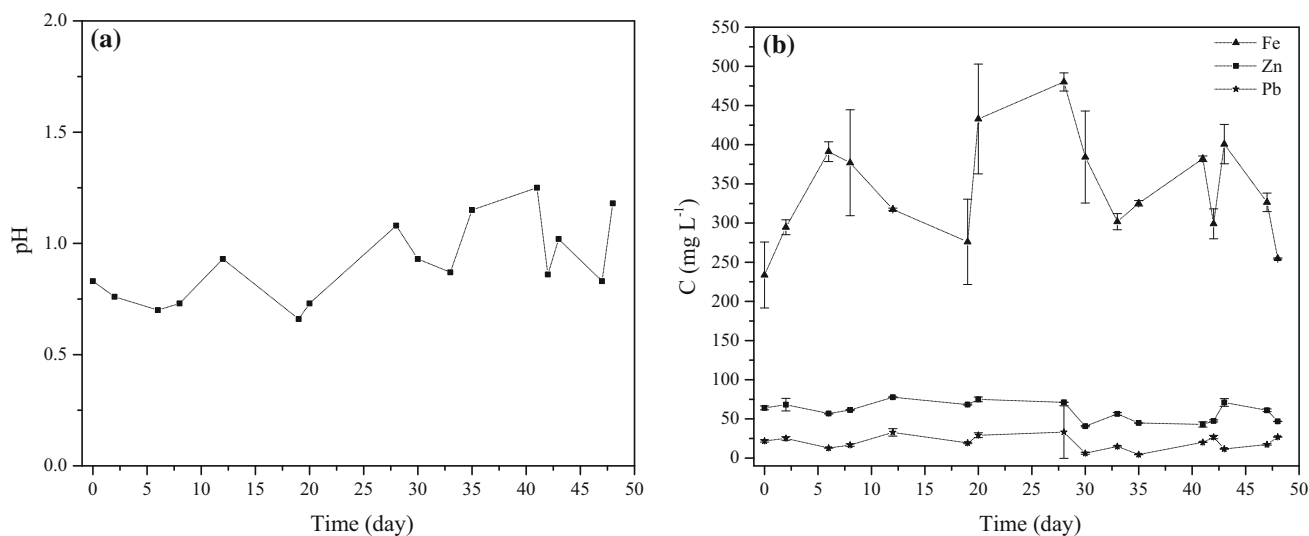
pH_{pzc}: point of zero charge

The results of pH_{pzc} for each adsorbent material are presented in Fig. 2, wherein for the FS material (Fig. 2a), a slightly alkaline character can be observed ($\text{pH}_{\text{pzc}} = 7.5$), as previously reported by the authors [27]. This result indicated a probable capability of removal of cations such as the observed heavy metals in the battery recycling industrial effluent. In addition, by observing the results for the DL mineral, a much more pronounced alkalinity was verified, achieving a $\text{pH}_{\text{pzc}} = 12.1$. This basic characteristic of the dolomite was already reported elsewhere [14, 28].

Table 1 Elemental characterization of the battery recycling industrial effluent

Element	Industrial wastewater			Legislated content limits (mg L ⁻¹) CONAMA
	IL (mg L ⁻¹)	$\bar{C} \pm SD$	SL	
S	5053	7613 ± 2273	9420	–
Cl	4	22 ± 22	40	–
K	5	7 ± 2	10	–
Ca	142	200 ± 87	326	–
Ti	1.0	1.2 ± 0.2	1.5	–
Cr	1	2 ± 1	3	1
Mn	0.5	1 ± 1	2	1
Fe	255	344 ± 96	480	15
Ni	2	1 ± 1	1	2
Cu	1	2 ± 1	3	1
Zn	45	60 ± 17	78	5
As	0.03	0.06 ± 0.05	0.09	0.5
Br	1	3 ± 1	4	1
Ba	1.1	1.1 ± 0.02	1.2	5
Pb	5	22 ± 15	33	0.5

CONAMA Conselho Nacional do Meio Ambiente (National Council for the Environment) [26]; \bar{C} is the average element concentration (mg L⁻¹); SD is the standard deviation (mg L⁻¹); and IL and SL are the inferior and superior concentration limits (mg L⁻¹), respectively

**Figure 1** a pH values and b concentration of Fe, Zn and Pb metals of the industrial wastewaters during the 50-day period.

In turn, for the commercial resin, a $pH_{pzc} = 5.7$ value was found, indicating its acidic characteristics which can be related to the presence of sulfonic acid functional groups. Based on the above, in this study, the potential of heavy metals removal by materials with different acid–base characteristics was investigated.

Scanning electron microscopy–energy-dispersive X-ray spectroscopy (SEM–EDX)

In Fig. 3a, b the SEM micrographs obtained for the FS before and after the process are shown, wherein one may notice ordered sets of fibers in the FS *in natura* (Fig. 3a). After the process, the FS (Fig. 3b) presented the formation of a rough layer on its surface, which may be ascribed to a microprecipitation process of

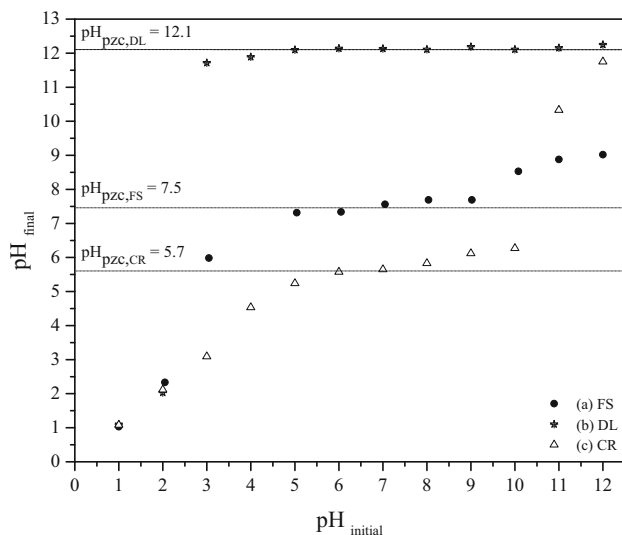


Figure 2 Point of zero charge (pH_{pzc}) of: a fish scales (FS), b mineral (DL) and c commercial resin (CR).

the metals on its surface. Furthermore, after the treatment process, the FS presented a gelatinous character and no longer exhibited the characteristic growth rings. Such behavior can be attributed to leaching of the inorganic phase (i.e., apatites) immersed within the organic phase (i.e., mostly composed of collagen), because of the strong acidity of the solution. The inorganic phase leaching from fish scales structure by acidic media was already reported elsewhere [27].

Regarding the mineral material, the DL micrographs (Fig. 3c) exhibited a fine powder together with agglomerates of particles of heterogeneous sizes and shapes. After the process (Fig. 3d), the DL presented an ordered structure. This may be due to the formation of a crystalline lattice, in which in the liquid phase formed this novel structure between the DL and the heavy metals in solution. Such crystalline structure can be related to the possibility of replacement of the original species in the DL constitution (Ca or Mg), which can be leached during the process, by the available metals from the aqueous phase (Fe, Zn, Pb) (see EDX and XRD results—Table 2 and “X-ray diffraction (XRD) analysis” section, respectively).

The micrographs for the CR showed its spherical shape and an extremely smooth surface (see Fig. 3e). The CR material presented a particle size distribution, in the range of $0.6 \text{ mm} < d_p < 0.8 \text{ mm}$, which can be observed for a Mag. 63 \times in Sup. Fig. S1. The CR surface indicated the absence of pores in its structure, confirmed by the textural parameters

(specific surface area of $1.532 \text{ m}^2 \text{ g}^{-1}$ and a total pore volume equal to $0.011 \text{ cm}^3 \text{ g}^{-1}$; data provided by the resin fabricant) which were low values when compared to most of the adsorbents. One may see that after the treatment process (Fig. 3f), the resin beads have been “cracked,” probably by the action of the strongly acidic media on the polymeric matrix of the CR material.

Table 2 shows the elemental composition of the three studied materials before and after the removal process. For the FS, the presence of C and O that may be related to both the organic phase (i.e., collagen) and inorganic phase (e.g., ascribed to the carbonated apatite $[\text{Ca}_{10}(\text{PO}_4)_6\text{CO}_3]$) of the scale can be observed. It is noteworthy that the percentage of inorganic species such as Mg and Ca decreased, most probably due to the action of acid pH and agreeing with the SEM results. The decrease in C, from carbonated apatite, was also indicative of leaching of the inorganic phase.

By analyzing the DL composition values, a high percentage of Ca, Mg and O from the dolomite structure was observed, which can be confirmed by FTIR and XRD techniques (“Fourier transform infrared (FTIR) spectroscopy” and “X-ray diffraction (XRD) analysis” sections). The same Mg and Ca leaching behavior can be observed for the mineral. In addition, a small amount of Si was found which was related to the impurities present in the mineral, in this case possibly silicates (e.g., SiO_2 , SiO_4) [16].

For the CR, a decrease in the Na cation after the treatment can be observed (see Table 2). This behavior can be ascribed to the ion exchange of the Na cation with the metallic ions in solution. The heavy metals were identified in the solid phase by the EDX analysis after the process for all investigated materials except for the Pb, which was not quantified. However, it must be highlighted that the EDX is a semiquantitative technique.

Fourier transform infrared (FTIR) spectroscopy

Infrared spectroscopy was performed on the fish scale, mineral and resin before and after their use in the process in order to identify possible changes in the structure of the materials, as shown in Fig. 4. Table 3 presents the summary of the observed IR absorption bands and the associated functional groups for the FS, DL and CR materials; also, the

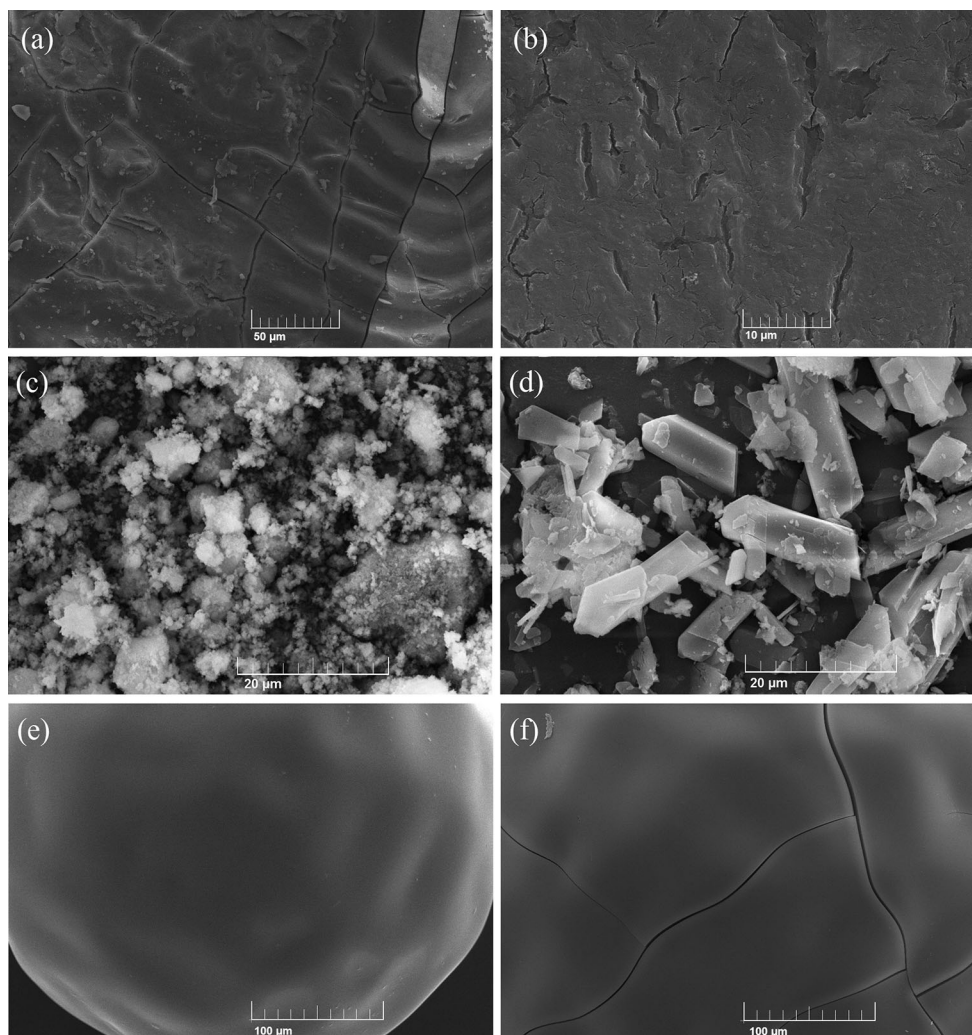


Figure 3 SEM images for **a** FS before (magnification $\times 2000$) and **b** FS after the process (mag. $\times 5000$); **c** DL before (mag. $\times 5000$) and **d** DL after the process (mag. $\times 5000$); **e** CR before (mag. $\times 750$) and **f** CR after the process (mag. $\times 750$).

Table 2 Overall chemical composition (%w/w) obtained by EDX spectrometry

Element	FS	FSAT	DL	DLAT	CR	CRAT
C	31.7	27.5	0.0	0.0	46.6	49.4
O	35.9	49.0	57.7	63.1	27.8	25.7
P	9.7	8.6	0.0	0.0	0	0
Si	0	0.0	2.1	0.0	0	0
Na	0.3	0.0	0.0	0.0	9.7	2.9
Mg	0.3	0.0	13.7	0.7	0	0
Ca	22.2	5.1	26.5	21.3	0	0
S	0	0.0	0.0	14.6	16.0	17.8
Fe	0	9.0	0.0	0.3	0	3.7
Zn	0	0.7	0.0	0.1	0	0.3

modifications on the IR bands after the process are presented in Table 4.

The IR spectra of fish scales *in natura* were reported in previous studies [27], wherein bands of amides (I, II and III) from collagen and PO_4^{3-} and CO_3^{2-} from the apatites were mainly observed. Similar bands were found by Marrakchi et al. [36]. By observing the IR spectra for the FS after the removal of the metals in acidic medium (Fig. 4b), overall the C–N bands of amide II and C–O of carboxylic acid can be observed due to the acid hydrolysis reaction of the collagen. The positive displacements in the bands corresponding to amides I and II (see Table 4) indicate the interaction of metals with the collagen structure. Since the decrease in the wavenumber is a consequence of the increase in the reduced mass [37], it can

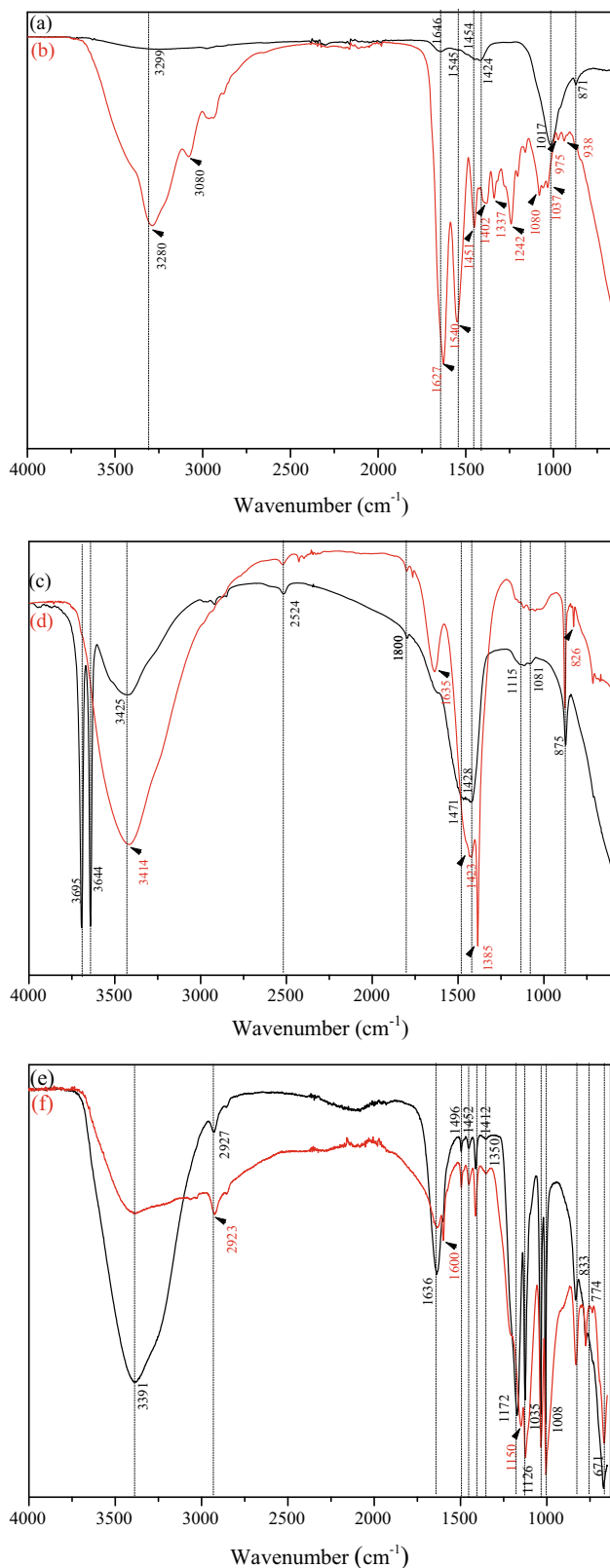


Figure 4 FTIR spectra for: (a) FS and (b) FS after the process; (c) DL and (d) DL after the process; (e) CR and (f) CR after the process.

be stated that the exchange of lighter species (i.e., H^+) by larger mass ones, such as the heavy metals in solution (Fe^{3+} , Zn^{2+} or Pb^{2+}), may have occurred.

By observing the FS spectra after the process (Fig. 4b; Table 4), a wide band between 3000 and 3600 cm^{-1} with a maximum intensity of 3280 cm^{-1} can be observed. Such a band can be attributed to the vibrations of amide stretching, from the scale structure, also to the water molecules adsorbed on the material after the process [30, 38]. After the process (see Fig. 4b), an arising band at 3080 cm^{-1} can be observed, which is probably associated with the Me^+ ion exchange by the proton from amide groups [29]. One may notice a band shifting from 1424 cm^{-1} , related to the CO_3^{2-} stretching, to 1402 cm^{-1} [27]. The modification in such a carbonate band was in accordance with the previously discussed EDX and SEM results, indicating the leaching of the inorganic phase in the acidic media. In addition, the band formed at 230 cm^{-1} also occurred due to the pH of the medium being very acidic [27], due to the collagen hydrolysis.

Moreover, several band shifts from 1646 to 1627, 1545 to 1540 and 1454 to 1451 cm^{-1} were observed, indicating that the amide and carbonate groups may act in the retention of the metal ions [39, 40]. The appearance of the 1337 cm^{-1} band probably indicates heavy metal interactions with the amino in the biosorption process, due to the acid hydrolysis of the collagen structure [33, 41].

The 1017 cm^{-1} band in the FS before the process was related to the phosphate groups (Fig. 5a). After contact with the acidic solution (Fig. 5b), this band was modified generating several bands: the shifting of bands to 1080 and 1037 cm^{-1} , and also the shifting to 975 and 936 cm^{-1} (duplet), which can be ascribed to the influence of phosphate in the retention of metal ions. The bands' displacements toward to lower wavenumber (975 and 936 cm^{-1} —positive shifting—see Table 4) can be associated with the higher reduced mass of the system due to the heavy metals retention onto the phosphate groups. On the other hand, the bands' displacements to higher wavenumber (1080 and 1037 cm^{-1} —negative shifting—see Table 4) are an indicative of the decrease in the reduced mass of the system, which can be ascribed to the phosphate leaching due to the acidic effect.

It must be highlighted that the evaluated system was a multicomponent one (i.e., Fe, Zn and Pb); thus, the three observed bands can be expected because

Table 3 Summary of IR absorption bands and the associated functional groups observed in the FS, DL and CR materials [29–35]

Sample	Wavenumber (cm ⁻¹)	Vibration	Functional group	Structure
FS	3299	N–H stretching	Amides I and II	Collagen
	1646	C–O bending	Amide I	Collagen
	1545	N–H bending and C–N stretching	Amide II	Collagen
	1454	C–N stretching and N–H bending	Pyrrole ring	Collagen
	1424	CO ₃ ²⁻ stretching	Carbonate	Carbonated apatite
	1017	PO ₄ ³⁻ stretching	Phosphate	Hydroxy, carbonated apatite
	871	CO ₃ ²⁻ stretching	Carbonate	Carbonated apatite
DL	3695 and 3644	O–H strong sharp	Hydroxyl	Water of hydration
	3425	O–H and CO ₃ ²⁻ stretching	Hydroxyl, carbonate	Water, magnesium carbonate
	2524	CO ₃ ²⁻ stretching	Carbonate	Calcium carbonate
	1800	CO ₃ ²⁻ stretching	Carbonate	Calcium carbonate
	1471 and 1428	HCO ₃ ⁻ stretching	Ionic carbonate bicarbonate	Magnesium carbonate
	1115 and 875	CO ₃ ²⁻ stretching	Carbonate	Calcium and Magnesium carbonate
	1081	Si–OH bond	Silicate	Silicate (impurities)
CR	3391	O–H bond	Sulfonate	Sulfonate
	2927	C–H	Alkanes	Polymeric matrix
	1636	C–C stretching	Phenyl ring	Divinylbenzene styrene polymeric matrix
	1035	C–C skeletal cis conformation	Alkanes	Polymeric matrix
	1496, 1452 and 1412	C=C stretching	Phenyl ring	Divinylbenzene styrene polymeric matrix
	1412 and 1126	S=O asymmetrical and symmetrical vibration	Sulfonate	Ion exchange sulfonate
	1350	S=O axial vibration	Sulfonate	Ion exchange sulfonate
	1172 and 671	C–S bending	Sulfonate	Ion exchange sulfonate
	1035, 1008 and 833	CH _{α,α'} out-of-plane bending and C _α = C _{α'} torsion; ring CH deformation	Phenyl ring	Divinylbenzene styrene polymeric matrix
	774	C–H out-of-plane bending vibrations	Phenyl ring	Divinylbenzene styrene polymeric matrix

each metal interaction may result in a different wavenumber. According to Nadeem et al. [41], phosphate groups commonly present a wide absorption range between 950 and 1100 cm⁻¹, wherein such shifting behavior was probably associated with the complexation of phosphate groups by coordination with metal ions. In addition, an ion exchange mechanism also may have occurred. According to Michalak et al. [42], in a biosorption process several groups might participate in the metal ion binding depending on the solution's pH value (e.g., carboxyl—pH = 2 to 5; carboxyl and phosphate—pH = 5–9). Hence, in a biosorption process, protons or light metal cations (e.g., Na⁺, K⁺, Mg²⁺, Ca²⁺) which are naturally bound to these functional

groups on the surface of the biosorbent may act as cation exchangers with the heavy metals available in solution.

Considering the pH_{pzc} value of the FS (pH_{pzc,FS} = 7.5—see Fig. 2a) and the acidic conditions of the studied system, one may notice that the FS surface will remain positively charged due to the proton's excess. At these pH conditions the ion exchange between the H⁺ and the Meⁿ⁺ will be propitious. The ion exchange hypothesis is in accordance with the results of Al Lafi and Abdullah [29]. The authors suggest that ion exchange reaction occurs during the metal ion uptake process (i.e., nH⁺ + Meⁿ⁺ ↔ Meⁿ⁺ + nH⁺), where H⁺ refers to an exchangeable proton in the solid surface. Therefore,

Table 4 Modifications of the IR spectra bands of FS, DL and CR materials after the process [29–35]

Sample	Modifications (cm ⁻¹)	Functional group
FS	3080 → arising band	N–H—amides I and II
	1646 → 1627 ($\Delta = 19$ —shifting)	C–O—amide I
	1545 → 1540 ($\Delta = 5$ —shifting)	N–H and C–N—amide II
	1454 → 1451 ($\Delta = 4$ —shifting)	C–N and N–H—pyrrole ring
	1424 → 1402 ($\Delta = 21$ —shifting)	CO ₃ ²⁻ —ionic carbonate
	1337 → arising band	C–N amine II—hydrolysis
	1230 → arising band	C–O carboxylic acid—hydrolysis
	1017 → 1080 ($\Delta = -63$); and	PO ₄ ³⁻ —ionic phosphate
	1017 → 1037 ($\Delta = -20$)—negative shifting	
	1017 → 975 ($\Delta = 42$); and	PO ₄ ³⁻ —ionic phosphate
	1017 → 936 ($\Delta = 81$)—positive shifting	
DL	3425 → 3414 ($\Delta = 11$ —shifting and bands' increase)	O–H—ion exchange in the H ⁺ group protonated by the metal
	1635 → bands' increase	C–O—carbonate
	1471 → 1423 ($\Delta = 48$ —shifting)	HCO ₃ ⁻ —ionic carbonate
	1428 → 1385 ($\Delta = 43$ —shifting)	HCO ₃ ⁻
	826 → arising band	Me ⁺ CO ₃ ²⁻ —ionic carbonate
CR	3391 → bands' decrease	O–H—sulfonate
	2927 → 2923 ($\Delta = 5$ —shifting)	C–C—alkanes
	1600 → arising bands	C–C—phenyl ring
	1126, 1035 and 1008 → bands' increase	S=O—sulfonate; C–C—alkanes
	833 and 671—bands' increase	C=C—phenyl ring; C–S—sulfonate
	1172 → 1150 ($\Delta = 22$ —shifting)	C–S—sulfonate

both the organic (collagen—i.e., amino, amide, hydroxylic and carboxylic functional groups) and inorganic phase (apatites—i.e., carbonate and phosphate) (see Table 4) may be involved in the biosorption process since these groups may act as ion exchangers, since $\text{pH} < \text{pH}_{\text{pzc}}$ [43].

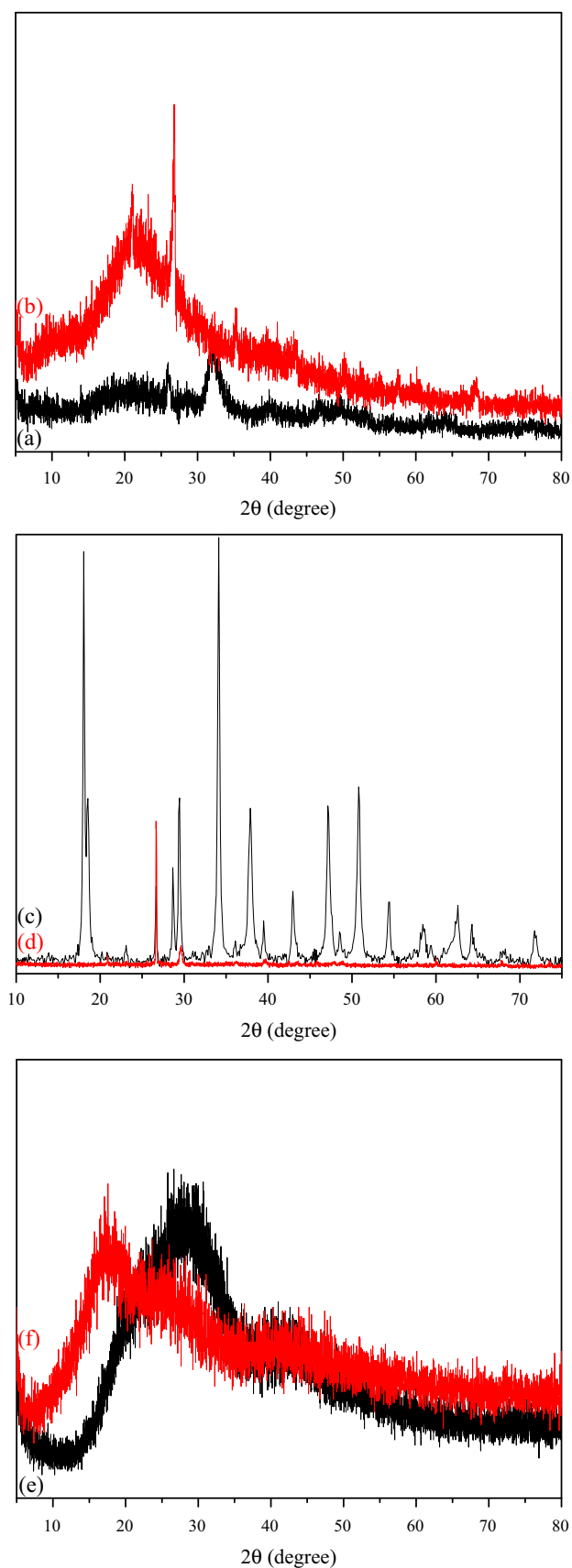
In addition, the substantial Ca decrease (see EDX results—Table 2) along with the phosphate group IR band displacements suggest that ion exchange between Ca²⁺ and the metals (Fe, Zn and Pb) was also involved in the complex mechanism of heavy metals removal for the FS.

In general, the IR analysis before and after the process indicated several modifications between the spectra; those results indicated a complex mechanism involving both ion exchange between amide, phosphate and carbonate groups of FS and the heavy metals. A similar complex mechanism was observed for biosorption of heavy metals by fish scales in the literature, namely for Cu(II) ions by Uzunoglu et al. [44] and for Pb(II) by Nadeem et al. [41]. In addition, after the process the FS presented a gelatinous character and a reddish color, which can be ascribed to

the apatites' leaching, collagen hydrolysis and Fe species assimilation in the FS structure. Therefore, the FS process is ruled by a very complex mechanism in the heavy metals adsorption including ion exchange, adsorption, microprecipitation and complexation. Such behavior is typical for biosorption processes [22, 23] due to the heterogeneity of functional groups on the surface.

In general, the DL spectra (Fig. 4c) present bands of calcium and magnesium hydroxide, hydroxyl (bound water), carbonate and bicarbonate characteristics of the dolomite structure, and impurities such as silicates can be observed.

By analyzing the DL spectra (Fig. 4c), two fine and intense bands at 3695 and 3644 cm⁻¹ corresponding to calcium and magnesium hydroxide can be observed [45]. A band at 3425 cm⁻¹ is related to the presence of hydroxyl groups (–OH) of bound water [28]. IR band is also observed at 2524 cm⁻¹ due to the presence of CaCO₃. The 1800 and 875 cm⁻¹ bands are assigned to the carbonate groups (CO₃²⁻) [46, 47]. In addition, at 1471 cm⁻¹ we see an absorption band corresponding to the C–O bond also from carbonates



◀ **Figure 5** XRD pattern of the: (a) FS before and (b) FS after the process; (c) DL before and (d) DL after the process; (e) CR before and (f) CR after the process.

[48]. The 1428 cm^{-1} band can be attributed to HCO_3^- , and the calcium and magnesium carbonate band was observed at 1115 cm^{-1} [49]. At 1081 cm^{-1} is a band corresponding to Si–OH binding [28].

In comparison, for the IR spectra of DL after the removal process (Fig. 4d), changes in some bands that can indicate the interaction between the metals and the functional groups acting as active sites in the mineral were observed, due to the ion exchange or the chemical precipitation of the heavy metals. This mineral material is a double salt; when in contact with water, a phenomenon of dissolution and hydration may occur. The charge of the surface is therefore the consequence of the formation of the ionic system for the solid–liquid interface, which is a function of pH. Below the pH_{pzc} , the mineral surface remains positively charged caused by a high concentration of the positively charged species [50]. These changes are reflected in the band stretching at 3414 cm^{-1} , which can be attributed to the interaction of the heavy metals with the hydroxyl group (OH), which can be involved in ion exchange process as well as observed for the FS; besides, this band modification may be an indicator of the formation of hydroxides with the available heavy metals (i.e., $\text{Me}(\text{OH})_x$ —where $\text{Me} = \text{Fe}, \text{Zn}$ or Pb ; as well as coordination complexes $\text{Me}(\text{H}_2\text{O})_x(\text{OH})_y$). A red-brown color of the precipitates formed in the solution after the treatment process was observed, which is related to the Fe(III) complex. Hence, the observed shifting may suggest that the hydroxyl functional groups are directly involved in interactions with the metals to form surface complexes [51]. Considering the highly alkaline characteristic of the DL ($\text{pH}_{\text{pzc}} = 12.1$ —see Fig. 2) and the consequent expressive pH change during the process (pH from 1 to 8—see Table 2), precipitation of the metals is most likely [52]. The intensities of the bands representing the CO_3^{2-} group increased to 1635, 1385, 1423 and 1385 cm^{-1} , which could be attributed to the insertion of metal ions that may have substituted for the HCO_3^- ions [28, 53], via ion exchange process [29].

In general, the observed changes of DL after the process (positive displacements and the intensity increase of the bands) indicate the influence of the

carbonate groups in the metal uptake, wherein the ion exchange between the cations from the original structure of the dolomite (i.e., Ca^{2+} , Mg^{2+}) by the heavy metals (Fe^{3+} , Zn^{2+} and Pb^{2+}) take place.

Figure 4e shows the IR spectra for the CR where bands ascribed to sulfonate, alkanes and phenyl ring were mainly observed, characteristic of the functional groups (sulfonic acids) and the polymeric matrix of the resin (divinylbenzene styrene).

By analyzing Fig. 4e, the band at 3391 cm^{-1} is related to the hydroxyls groups, 2927 cm^{-1} the C–H bond from alkanes, 1636 cm^{-1} the ring C–C stretch of phenyl derived from the divinylbenzene styrene polymeric matrix of the resin and 1035 cm^{-1} to C–O bonds [33, 54–56]. In addition, the IR band 1008 cm^{-1} can be ascribed to $\text{CH}_{\alpha,\alpha'}$ out-of-plane bending and $\text{C}_{\alpha} = \text{C}_{\alpha'}$ torsion, and the absorption band in 833 cm^{-1} is related to the ring CH deformation, both associated with the phenyl ring, from the divinylbenzene styrene polymeric matrix of the resin [30, 33]. The aromatic ring structure C=C bonds of the resin polymer backbone can be also observed in three other bands at 1496, 1452 and 1412 cm^{-1} [33, 55] as well as the out-of-plane bending vibrations at 774 cm^{-1} [33]. The bands at 1172 and 671 cm^{-1} were observed due to the C–S bond [30, 33], together with the 1126 and 1412 cm^{-1} bands related to asymmetrical and symmetrical S=O vibration and a 1350 cm^{-1} band related to the S–O axial vibration [56], which all confirm the presence of sulfonate groups in the resin.

After the removal process (Fig. 4f), one may notice mainly changes in the sulfonate group (see Table 4). The positive shifting (from 2927 to 2923 cm^{-1} , and from 1172 to 1150 cm^{-1}) as well as the intensity increase of the bands (at 1126 , 1035 , 1008 , 833 and 631 cm^{-1}) related to S=O, C–S, C=C e C–C can be all consequence of the heavy metals interaction with the sulfonic groups, thus affecting the whole bond chain. These modifications point out the interactions in the sulfonate groups that can be related to ion exchange between the Na^{+} in this functional group and the heavy metals in solution [29]. The substantial decrease in the Na concentrations in the CR after the process with the concomitant increase in the heavy metals concentrations (see Table 5) is in accordance with these results and evidences the ion exchange between such cations.

X-ray diffraction (XRD) analysis

The FS, DL and CR material diffractograms before and after the process are shown in Fig. 5. Regarding the FS (Fig. 5a), results similar to those reported by Ribeiro et al. [27] were obtained, indicating the presence of a characteristic halo from amorphous structures of organic phases, corresponding to the collagen, and also a peak at 32° relative to the inorganic phase of apatites, thereby confirming both phases as previously discussed in the FTIR and SEM–EDX results. After its use in the process (Fig. 5b), a significant increase in the halo in the region from $2\theta = 15^{\circ}$ to 25° related to the amorphous organic phase [57] was observed due to the contact with the acidic medium. This result confirms the leaching of the inorganic phase that led to enhanced collagen phase exposure. In addition, the disappearance of the inorganic phase peak (32°) is corroborated with the inorganic species removal from the FS structure [40]. Finally, the new intense peak at 27° may be related to the presence of heavy metals after the removal process. Since Fe presented the highest concentrations in the effluent ($C_{\text{Fe}} = 344 \pm 96\text{ mg L}^{-1}$), the presence of this peak can probably be attributed to iron structures. According to Parga et al. [58], the peak at 27° is related to the iron (III) oxide–hydroxide (i.e., anhydrous— $\text{Fe}(\text{OH})_3$; and its hydrated form— $\text{Fe}(\text{H}_2\text{O})_3(\text{OH})_3$), which is much more likely for pH values higher than 4. This result as well as the reddish precipitate observed after the treatment process ratifies the FTIR results.

For the DL mineral before the process (Fig. 5c), characteristic peaks of $\text{Ca}(\text{OH})_2$ were observed at 18° , 28° , 34° , 47° , 51° and 55° [46]. Moreover, the peaks at 38° and 58° correspond to $\text{Mg}(\text{OH})_2$ and at 29° and 40° to CaCO_3 [14, 45]; the hydroxides appearance in the dolomite structure is related to its hygroscopicity. At last, the peaks at 21° and 26° indicated the presence of SiO_2 (JCPDS database No: 36-0426 dolomite). In general, the observed peaks confirm that this mineral material consisted of dolomitic lime as the main composition along with other impurities, confirming the FTIR and SEM–EDX results. After its use in the process (Fig. 5d), few peaks remained in the diffractogram, indicating changes in its crystalline structure. The appearance of an intense peak at 27° may indicate the interaction of the material with the metal ions, resulting in novel structures, such as carbonates [17]. It must be highlighted that the same

Table 5 Elemental characterization of the synthetic effluent (SEF) before the treatment and the synthetic effluent treated by the different adsorbent materials (SEFT)

Element	SEF (mg L ⁻¹)	SEFT		
		FS (mg L ⁻¹)	DL (mg L ⁻¹)	RC (mg L ⁻¹)
Na	374	734	711	19343
Mg	8	15	116	3
P	2	124	0	0
S	7	0	4	21
Cl	4	91	9	6
K	8	17	3	11
Ca	0.2	149	3721	4
Cr	1	0	0.1	0.1
Mn	1	4	0.4	0.09
Fe	390	183	196	1
Cu	2	1	0.02	0.5
Zn	54	21	26	2
Ag	2	1	3	2
Ba	2	3	0.5	1
Pb	27	8	9	0.02
pH value	1	5	8	1

peak was observed for FS and DL, which can probably be related to the precipitation of heavy metals for these two alkaline materials [59]. The peak at 29° is associated with calcium oxide, indicating that this compound remained in the DL structure after the process. This result was probably related to the lower solubility of Ca (0.013 g L⁻¹ at 25 °C) when compared to Mg (0.139 g L⁻¹ at 25 °C) [60]. The XRD results were in accordance with the decrease in magnesium content after the process by EDX (Table 2), indicating that magnesium was leached to the solution, while calcium remained in the solid phase while interacting with cations in solution. In general, the changes in the diffractograms indicated the disappearance of the majority of the peaks corresponding to the hydroxides, following the formation of new complexes with the entrance of the metals.

The XRD analysis for the CR showed typical diffractograms of polymer samples (see Fig. 5e–f), wherein a characteristic halo of amorphous polymer material is identified between 20° and 30° [19, 20, 61, 62]. After the metal removal process, a peak appeared at 17° indicating the metal ion entry, probably related to the ion exchange of Na⁺ in the sulfonate groups with the heavy metals in solution.

Therefore, by analyzing the XRD along with the FTIR and SEM–EDX results for all the three evaluated materials, it can be concluded that different mechanisms (e.g., precipitation, complexation, adsorption,

ion exchange) may rule the heavy metals removal depending on its physicochemical characteristics. In addition, one may notice that for all evaluated materials, leaching and loss of mass were observed, indicating a chemical and physical instability due to the extremely acidic characteristic of the effluent, which is commonly a key factor regarding the adsorption processes as the solution's pH significantly influences its performance.

Kinetic experiments

In order to evaluate the efficiency of the adsorbent materials of different characteristics in the removal of metals from solution, laboratory-scale experiments were conducted. The tests were carried out by using the mineral adsorbent (DL), the tilapia fish scales (*Oreochromis niloticus*) (FS) and the Amberlite IR120 ion exchange resin (CR) with a synthetic effluent based on the pH and the concentrations of the heavy metals observed at higher concentrations (Fe, Zn, Pb) in the industrial effluent. Thus, the synthetic effluent used in these tests was prepared with the following characteristics: $C_{Fe,0} = 400 \text{ mg L}^{-1}$, $C_{Zn,0} = 60 \text{ mg L}^{-1}$, $C_{Pb,0} = 30 \text{ mg L}^{-1}$ and pH = 1.

The kinetics of heavy metals removal (Fe, Zn, Pb) employing the different adsorbents are shown in Fig. 6. All the assessed materials were capable of removing the heavy metals from the liquid phase,

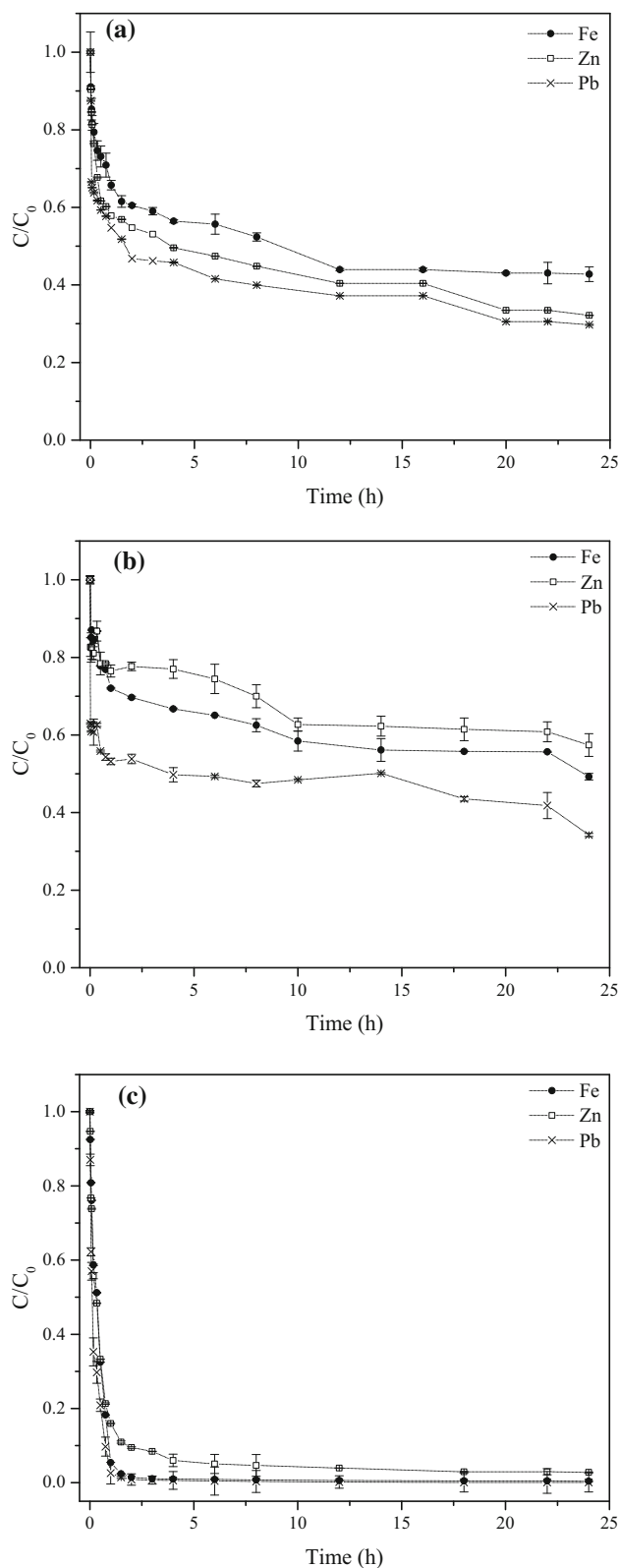


Figure 6 Kinetics of Fe, Zn and Pb metal removal from synthetic effluent by using: **a** FS; **b** DL; and **c** CR. Experimental conditions: $\text{pH}_{\text{initial}} = 1$, $T = 30\text{ }^\circ\text{C}$ and $m_{\text{ads}} = 20\text{ g}$.

especially the CR which reached values almost equal to zero. The percentage of removal achieved by the end of the process was as follows for the same initial mass of each adsorbent material: $\%R_{\text{Fe}} = 55\%$, $\%R_{\text{Zn}} = 67\%$ and $\%R_{\text{Pb}} = 69\%$ for the FS; $\%R_{\text{Fe}} = 48\%$, $\%R_{\text{Zn}} = 43\%$ and $\%R_{\text{Pb}} = 67\%$ for the DL; and $\%R_{\text{Fe}} = 99\%$, $\%R_{\text{Zn}} = 96\%$ and $\%R_{\text{Pb}} = 99\%$ for the CR. In addition, by analyzing Fig. 6a–c, one may observe that the CR showed the most favorable kinetics among the evaluated materials, achieving an equilibrium time within 2.5 h, followed by DL (10 h) and FS (12 h).

A comprehensive elemental characterization of the liquid phase (before and after the treatment—i.e., 24 h) was performed by applying each adsorbent material in order to investigate the phase migration of the species (see Table 5) and in an attempt to clarify the mechanisms involved for each material as well as to assess the quality of the generated water after the process. All materials removed some of the heavy metals, but the CR was the only one that achieved levels below the legislated limits for the heavy metals focused on in this study (i.e., 15, 5 and 0.5 mg L^{-1} for Fe, Zn and Pb, respectively—CONAMA [26], Norm 357/2005). In addition, for other potentially harmful species (e.g., Cr and Cu), low values were also achieved for the adsorbents. The elemental characterization also showed leaching of elements for each adsorbent. For instance, for the fish scales, an increase in the Ca, P, Na and Cl, related to the mineral phase leaching (e.g., hydroxyapatites, carbonated apatite and chlorapatite) was also observed in SEM–EDX and FTIR analyses. For the DL material, an increase was observed for Ca, Mg and Na, also characteristic of the dolomite material. In other words, the increase in Ca and Mg in the final solution is justified because these cations are relatively soluble in aqueous medium. Finally, for the CR, an intense increase in Na was observed related to the ion exchange of Na^+ with the metals in solution, as previously discussed. These results are in accordance with the characterization techniques (i.e., FTIR and XRD). Hence, the Na^+ released by the CR was ascribed to the fact that this material is an acidic ion exchanger. It must be highlighted that the TXRF technique presents restrictions in the quantification of species with atomic number below Al ($Z < 13$); thus, the observed Na^+ values are only an estimate (i.e., semiquantitative).

In addition, in Table 5 the values of the pH in the aqueous medium are presented, in which a neutralization was observed by using FS and DL materials, achieving final pH values of 5 and 8, respectively. For both fish scales and mineral adsorbents, the observed increase in the pH values after the removal process was associated with the release of the species in solution, making the medium more basic. For FS material, a release of P was observed during the treatment process due to the presence of PO_4^{3-} in the inorganic structure of the apatites. It must be noted that elevated levels of P in a discharging effluent could lead to eutrophication of aquatic systems [63]. However, for the resin the pH values of the solution remained the same as the initial value ($\text{pH} = 1$). In this way, although the CR presented the best heavy metals removal capacity, this material did not provide a neutral effluent and could demand further neutralization. Hence, the pH stability observed for the treatment process with the CR was most probably associated with ion exchange between the exchanger cation (Na^+) and the heavy metals, keeping the pH of the medium stable. However, this was the cause of the high removal yields observed, since even for extremely acidic pH values, as in this case, the functional groups (i.e., sulfonic acids) of the resin have been mostly in their dissociated form (conjugated base—sulfonate— SO_3^-) taking into account the pK_a value of sulfonic acid ($\text{pK}_a = 2.7$) [64]. Hence, the high adsorption capacity for the cations in solution can be explained by intense electrostatic interactions with the resin functional groups. Another piece of evidence was the intense release of Na^+ ions to the solution during the process, indicating the exchange between such ions and the heavy metals of the effluent.

In general, the CR presented an excellent capacity for heavy metals removal; however, it was inefficient for neutralization of the effluent compared to the FS and DL, which were capable of achieving values of pH within the legislated limits.

In addition to the elemental characterization in the liquid phase the remaining solid phase (sludge) after the process was also characterized in terms of its elemental composition as shown in Table 6.

By analyzing the composition of chemical elements in the solid phase, it was possible to identify the heavy metals (Fe, Zn and Pb) transferred from the solution to the adsorbent during the treatment processes for all the FS, DL and CR adsorbent materials.

Table 6 Elemental characterization of the different adsorbent materials before treatment and of the sludge generated after the treatment processes

Element	Concentration (mg g^{-1})					
	FS	FSAT	DL	DLAT	CR	CRAT
Na	4082	1349	0	564	17019	2150
Mg	46	24	692	563	2	3
P	935	140	11	1	33	34
S	1294	340	0	6	110	95
Cl	62	99	0	3	4	2
K	4	22	8	10	51	1
Ca	10	39	2742	799	12	4
Cr	1	1	0	1	1	1
Mn	1	6	1	2	0	1
Fe	13	212	13	284	15	319
Cu	0	2	0	0	1	1
Zn	0	45	0	21	2	47
Ag	11	0	19	0	2	3
Ba	3	4	1	0	6	2
Pb	0	16	0	18	0	29
Sludge mass (g)	20	10	20	14	20	11

AT—after the treatment process (e.g., FSAT—fish scales after the treatment)

Regarding the sludge mass remaining at the end of the process, DL generated the largest amount of sludge, namely 14 g (70%). In turn, the FS reduced its mass by half resulting in 10 g (50%); the reduction in mass can be associated with the observed leaching of the inorganic phase (as already discussed in the previous sections). This result is in accordance with the organic/inorganic phase composition in fish scales, generally around 50/50 (%w/w), as reported elsewhere [65, 66]. In this sense, it must be concluded that the 50% mass reduction relates to the complete leaching of the inorganic phase from the FS composition. Finally, for the CR, a final sludge mass of 11 g (55%) was observed, which was related to the extremely acidic pH of the medium causing significant resin mass decrease (as observed in the SEM images by its cracked aspect—Fig. 3f) and was justified by the appearance of S and Na in large amounts in the liquid phase after the process. The great amounts of sludge generated remain a significant problem since it leads to disposal costs. Therefore, minimization of the sludge must be considered as a key factor.

On the basis of the results obtained from this study it was possible to verify the following: (1) the

adsorbents tested were capable of removing the Fe, Zn and Pb heavy metals from a synthetic effluent, even in a multicomponent and complex system prepared on the basis of the characteristics of an industrial effluent; (2) the CR showed the highest capacity to remove metals from the liquid phase; (3) leaching of the mineral adsorbent and inorganic phase of the fish scales took place in the process, which led to the medium neutralization; (4) the process of heavy metals removal by using the fish scales and the mineral adsorbent was not solely phenomenologically described by an adsorption phenomenon, but by a much more complex process involving other simultaneous mechanisms in the neutralization and heavy metals removal (e.g., ion exchange, surface complexation and precipitation).

In the present study, the kinetic data along with the physical, chemical and morphological characterization of the adsorbents (before and after the process) indicate that the materials present a great potential as agents in the removal of heavy metals loading and neutralization, except for the resin which did not change the pH values of automotive battery effluents.

At last, since each adsorbent material presented different characteristics in terms of neutralization and heavy metals removal capacity, the possibility of a hybrid process could be a likely adequate alternative. In other words, a pre-neutralization by applying the fish scales or the dolomite could be followed by heavy metals removal using the ion exchange resin because of its great capacity for removal including the possibility of regeneration.

Conclusions

The physicochemical and elemental characterization of the automotive battery recycling industry effluent revealed it to be a complex and strongly acidic effluent mainly constituted of a variety of heavy metals above the legislated limits for discharge (e.g., Fe, Zn, Pb). Regarding the feasibility of the adsorbent materials studied (fish scales, mineral dolomite and commercial resin), different capacities in the removal of the heavy metals were observed for each material, namely $CR > FS > DL$. In addition, different neutralization capacities of the effluent were observed, in which the DL and FS materials achieved the pH standards for discharge ($5 < \text{pH} < 9$), but the CR did not change the pH value of the effluent, despite an

excellent heavy metals removal capacity. The differing characteristics of each material were assessed through a comprehensive physicochemical and morphological characterization, which was helpful in the elucidation of the phenomena involved in the process (i.e., for CR, mainly, ion exchange, whereas for FS and DL, a much more complex mechanism was observed including leaching of species from the adsorbent materials with concomitant ion exchange, surface complexation and precipitation of the heavy metals). The characterization also allowed us to observe a chemical and physical instability for all materials due to the highly acidic values of the battery effluent. The leaching and sludge generation were quantified, in which the DL presented the highest sludge generation. Thus, despite the traditional use of dolomite in the chemical precipitation of the effluent in the industry, the excessive sludge generation would lead to additional costs for disposal. In this sense, the results of this work indicate that the use of hybrid processes by applying combinations of these adsorbent materials (e.g., DL and FS; DL and CR) can provide a higher-quality treated effluent in conjunction with a lower sludge generation. Therefore, the associated use of the materials, targeting both an effective removal of the heavy metals in solution and the effluent neutralization, could be a simple and cost-effective alternative.

Acknowledgements

The authors are very grateful to National Council for Scientific and Technological Development (CNPq) for the financial support of this study (Grant Number 480107/2013-0).

Electronic supplementary material: The online version of this article (<https://doi.org/10.1007/s10853-018-2150-6>) contains supplementary material, which is available to authorized users.

References

- [1] Bahadir T, Bakan G, Altas L, Buyukgungor H (2007) The investigation of lead removal by biosorption: an application at storage battery industry wastewaters. *Enzyme Microb Technol* 41:98–102

- [2] Needleman H (2004) Lead poisoning. *Annu Rev Med* 55:209–222
- [3] Gottesfeld P, Cherry CR (2011) Lead emissions from solar photovoltaic energy systems in China and India. *Energy Policy* 39:4939–4946
- [4] Feng Y, Wang Y, Wang Y et al (2017) Simple fabrication of easy handling millimeter-sized porous attapulgite/polymer beads for heavy metal removal. *J Colloid Interface Sci* 502:52–58
- [5] Sun Z, Cao H, Zhang X et al (2017) Spent lead-acid battery recycling in China—a review and sustainable analyses on mass flow of lead. *Waste Manag* 64:190–201
- [6] Quiterio SL, Moreira FR, Da Silva CRS et al (2006) Avaliação da poluição ambiental causada por particulado de chumbo emitido por uma reformadora de baterias na cidade do Rio de Janeiro, Brasil (in Portuguese). *Cad Saude Publica* 22:1817–1823
- [7] Milanez B, Bührs T (2009) Capacidade Ambiental e Emulação de Políticas Públicas: O Caso da Responsabilidade Pós-Consumo Para Resíduos de Pilhas e Baterias no Brasil (in Portuguese). *Planej e Políticas Públicas* 33:257–289
- [8] Abdolali A, Ngo HH, Guo W et al (2017) Application of a breakthrough biosorbent for removing heavy metals from synthetic and real wastewaters in a lab-scale continuous fixed-bed column. *Bioresour Technol* 229:78–87
- [9] Maruthamuthu S, Dhanibabu T, Veluchamy A et al (2011) Electrokinetic separation of sulphate and lead from sludge of spent lead acid battery. *J Hazard Mater* 193:188–193
- [10] Ambrose H, Gershenson D, Gershenson A, Kammen D (2014) Driving rural energy access: a second-life application for electric-vehicle batteries. *Environ Res Lett* 9:94004
- [11] Pehlivan E, Özkan AM, Dinç S, Parlayici Ş (2009) Adsorption of Cu²⁺ and Pb²⁺ ion on dolomite powder. *J Hazard Mater* 167:1044–1049
- [12] Reichert J, Binner JGP (1996) An evaluation of hydroxyapatite-based filters for removal of heavy metal ions from aqueous solutions. *J Mater Sci* 31:1231–1241. <https://doi.org/10.1007/BF00353102>
- [13] Padilla-Ortega E, Leyva-Ramos R, Flores-Cano JV (2013) Binary adsorption of heavy metals from aqueous solution onto natural clays. *Chem Eng J* 225:536–546
- [14] Salameh Y, Albadarin AB, Allen S et al (2015) Arsenic(III, V) adsorption onto charred dolomite: charring optimization and batch studies. *Chem Eng J* 259:663–671
- [15] Wu M, Zhang J, Peng Y et al (2017) An investigation into mechanism of cation adsorption by reconstruction of calcined layered double hydroxide. *Microporous Mesoporous Mater* 242:182–189
- [16] Ghosh SN, Vishwanathan VN, Chatterjee AK (1976) Estimation of dolomite mineral in limestone by infra-red spectroscopy. *J Mater Sci* 11:1167–1170. <https://doi.org/10.1007/BF00553128>
- [17] Liu Z, Shen Q, Zhang Q et al (2014) The removal of lead ions of the aqueous solution by calcite with cotton morphology. *J Mater Sci* 49:5334–5344. <https://doi.org/10.1007/s10853-014-8236-x>
- [18] Farnane M, Tounsadi H, Elmoubarki R et al (2017) Alkaline treated carob shells as sustainable biosorbent for clean recovery of heavy metals: kinetics, equilibrium, ions interference and process optimisation. *Ecol Eng* 101:9–20
- [19] Bhatt RR, Shah BA (2015) Sorption studies of heavy metal ions by salicylic acid-formaldehyde-catechol terpolymeric resin: isotherm, kinetic and thermodynamics. *Arab J Chem* 8:414–426
- [20] Bento HBS, de Castro HF, de Oliveira PC, Freitas L (2017) Magnetized poly(STY-co-DVB) as a matrix for immobilizing microbial lipase to be used in biotransformation. *J Magn Magn Mater* 426:95–101
- [21] Liu B, Wang D, Xu Y, Huang G (2011) Adsorption properties of Cd(II)-imprinted chitosan resin. *J Mater Sci* 46:1535–1541. <https://doi.org/10.1007/s10853-010-4958-6>
- [22] Gadd GM (2009) Biosorption: critical review of scientific rationale, environmental importance and significance for pollution treatment. *J Chem Technol Biotechnol* 84:13–28
- [23] Fomina M, Gadd GM (2014) Biosorption: current perspectives on concept, definition and application. *Bioresour Technol* 160:3–14
- [24] Espinoza-Quiñones FR, Módenes AN, de Pauli AR, Palácio SM (2015) Analysis of trace elements in groundwater using ICP-OES and TXRF techniques and its compliance with Brazilian protection standards. *Water Air Soil Pollut* 226:32
- [25] Park J, Regalbuto JR (1995) A simple, accurate determination of oxide PZC and the strong buffering effect of oxide surfaces at incipient wetness. *J Colloid Interface Sci* 175:239–252
- [26] Brazil (2005) Norm 357/2005 (in Portuguese) published on the Union Official Newspaper of Brazil (18 March 2005), No. 53, pp 58–63. Brazilian Council of Environmental Quality Regulation—CONAMA
- [27] Ribeiro C, Scheufele FB, Espinoza-Quiñones FR et al (2015) Characterization of *Oreochromis niloticus* fish scales and assessment of their potential on the adsorption of reactive blue 5G dye. *Colloids Surf A Physicochem Eng Asp* 482:693–701
- [28] Albadarin AB, Mangwandi C, Al-Muhtaseb AH et al (2012) Kinetic and thermodynamics of chromium ions adsorption onto low-cost dolomite adsorbent. *Chem Eng J* 179:193–202
- [29] Al Lafi AG, Al Abdullah J (2015) Cesium and cobalt adsorption on synthetic nano manganese oxide: a two

- dimensional infra-red correlation spectroscopic investigation. *J Mol Struct* 1093:13–23
- [30] Colthup NB (1950) Spectra-structure correlations in the infra-red region. *J Opt Soc Am* 40:397
- [31] Derrick MR, Stulik D, Landry JM (1999) Infrared spectroscopy in conservation science. The Getty Conservation Institute, Los Angeles
- [32] Miller FA, Wilkins CH (1952) Infrared spectra and characteristic frequencies of inorganic ions. *Anal Chem* 24:1253–1294
- [33] Movasaghi Z, Rehman S, ur Rehman I (2008) Fourier transform infrared (FTIR) spectroscopy of biological tissues. *Appl Spectrosc Rev* 43:134–179
- [34] Nyquist RA, Kagel RO (1971) Infrared spectra of inorganic compounds. Handbook of infrared and raman spectra of inorganic compounds and organic salts, 1st edn. Academic Press, Michigan, pp 1–18
- [35] Smidt E, Meissl K (2007) The applicability of Fourier transform infrared (FT-IR) spectroscopy in waste management. *Waste Manag* 27:268–276
- [36] Marrakchi F, Ahmed MJ, Khanday WA et al (2017) Mesoporous carbonaceous material from fish scales as low-cost adsorbent for reactive orange 16 adsorption. *J Taiwan Inst Chem Eng* 71:47–54
- [37] Skoog DA, Holler FJ, Crouch SR, Douglas A, Skoog F, James Holler SRC (2007) Principles of instrumental analysis, 6th edn. Thomson Brooks/Cole, Belmont
- [38] Minamisawa M, Minamisawa H, Yoshida S, Takai N (2004) Adsorption behavior of heavy metals on biomaterials. *J Agric Food Chem* 52:5606–5611
- [39] Saber-Samandari S, Saber-Samandari S, Nezafati N, Yahya K (2014) Efficient removal of lead (II) ions and methylene blue from aqueous solution using chitosan/Fe-hydroxyapatite nanocomposite beads. *J Environ Manag* 146:481–490
- [40] He X, Che R, Wang Y et al (2015) Core-nanoshell magnetic composite material for adsorption of Pb(II) in wastewater. *J Environ Chem Eng* 3:1720–1724
- [41] Nadeem R, Ansari TM, Khalid AM (2008) Fourier transform infrared spectroscopic characterization and optimization of Pb(II) biosorption by fish (*Labeo rohita*) scales. *J Hazard Mater* 156:64–73
- [42] Michalak I, Chojnacka K, Witek-Krowiak A (2013) State of the art for the biosorption process—a review. *Appl Biochem Biotechnol* 170:1389–1416
- [43] Liu R, Liu H, Qiang Z et al (2009) Effects of calcium ions on surface characteristics and adsorptive properties of hydrous manganese dioxide. *J Colloid Interface Sci* 331:275–280
- [44] Uzunoğlu D, Özer A (2016) Adsorption of hazardous heavy metal copper(II) from aqueous effluents onto waste material fish (*Dicentrarchus labrax*) scales: optimization, equilibrium, kinetics, thermodynamic, and characterization studies. *Desalin Water Treat* 57:22794–22798
- [45] Correia LM, de Sousa Campelo N, Novaes DS et al (2015) Characterization and application of dolomite as catalytic precursor for canola and sunflower oils for biodiesel production. *Chem Eng J* 269:35–43
- [46] Mangwandi C, Albadarin AB, Glocheux Y, Walker GM (2014) Removal of ortho-phosphate from aqueous solution by adsorption onto dolomite. *J Environ Chem Eng* 2:1123–1130
- [47] Yoshida M, Koilraj P, Qiu X et al (2015) Sorption of arsenate on MgAl and MgFe layered double hydroxides derived from calcined dolomite. *J Environ Chem Eng* 3:1614–1621
- [48] Albadarin AB, Mo J, Glocheux Y et al (2014) Preliminary investigation of mixed adsorbents for the removal of copper and methylene blue from aqueous solutions. *Chem Eng J* 255:525–534
- [49] Ivanets AI, Kitikova NV, Shashkova IL et al (2016) Using of phosphatized dolomite for treatment of real mine water from metal ions. *J Water Process Eng* 9:246–253
- [50] Al-Degs YS, El-Barghouthi MI, El-Sheikh AH, Walker GM (2008) Effect of solution pH, ionic strength, and temperature on adsorption behavior of reactive dyes on activated carbon. *Dye Pigment* 77:16–23
- [51] Yang S, Guo Z, Sheng G, Wang X (2012) Application of a novel plasma-induced CD/MWCNT/iron oxide composite in zinc decontamination. *Carbohydr Polym* 90:1100–1105
- [52] Liang Z, Shi W, Zhao Z et al (2017) The retained templates as “helpers” for the spherical meso-silica in adsorption of heavy metals and impacts of solution chemistry. *J Colloid Interface Sci* 496:382–390
- [53] Mohammadi M, Ghaemi A, Torab-Mostaedi M et al (2015) Adsorption of cadmium (II) and nickel (II) on dolomite powder. *Desalin Water Treat* 53:149–157
- [54] Ciopec M, Negrea A, Lupa L et al (2014) Studies regarding As(V) adsorption from underground water by Fe-XAD8-DEHPA impregnated resin. Equilibrium sorption and fixed-bed column tests. *Molecules* 19:16082–16101
- [55] Singh AN, Singh S, Dubey VK (2013) Immobilization of procerain B, a cysteine endopeptidase, on amberlite MB-150 beads. *PLoS ONE* 8:e66000
- [56] Scheufele FB, Módenes AN, Borba CE et al (2016) Monolayer–multilayer adsorption phenomenological model: kinetics, equilibrium and thermodynamics. *Chem Eng J* 284:1328–1341
- [57] Zhou K, Yang Z, Liu Y, Kong X (2015) Kinetics and equilibrium studies on biosorption of Pb(II) from aqueous solution by a novel biosorbent: *Cyclosorus interruptus*. *J Environ Chem Eng* 3:2219–2228

- [58] Parga JR, Valenzuela JL, Munive GT et al (2014) Thermodynamic study for arsenic removal from freshwater by using electrocoagulation process. *Adv Chem Eng Sci* 4:548–556
- [59] Oliva J, De Pablo J, Cortina J-L et al (2010) The use of apatite IITM to remove divalent metal ions zinc(II), lead(II), manganese(II) and iron(II) from water in passive treatment systems: column experiments. *J Hazard Mater* 184:364–374
- [60] Atkins PW, Jones L, Laverman L (2016) *Chemical principles: the quest for insight*, 7th edn. W.H. Freeman, New York
- [61] Neves JS, De Souza FG, Suarez PAZ et al (2011) In situ production of polystyrene magnetic nanocomposites through a batch suspension polymerization process. *Macromol Mater Eng* 296:1107–1118
- [62] Masoumi A, Ghaemy M (2014) Adsorption of heavy metal ions and azo dyes by crosslinked nanochelating resins based on poly(methylmethacrylate-co-maleic anhydride). *Express Polym Lett* 8:187–196
- [63] Correll DL (1998) The role of phosphorus in the eutrophication of receiving waters: a review. *J Environ Qual* 27:261
- [64] Monte Blanco SPD, Scheufele FB, Módenes AN et al (2017) Kinetic, equilibrium and thermodynamic phenomenological modeling of reactive dye adsorption onto polymeric adsorbent. *Chem Eng J* 307:466–475
- [65] Villanueva-Espinosa JF, Hernandez-Esparza M, Ruiz-Trevino FA (2001) Adsorptive properties of fish scales of *Oreochromis Niloticus* (Mojarra Tilapia) for metallic ion removal from waste water. *Ind Eng Chem Res* 40:3563–3569
- [66] Ikoma T, Kobayashi H, Tanaka J et al (2003) Microstructure, mechanical, and biomimetic properties of fish scales from *Pagrus major*. *J Struct Biol* 142:327–333